

Piotr Smarzewski

Lublin University of Technology, Faculty of Civil Engineering and Architecture, ul. Nadbysztycka 40, 20-618 Lublin, Poland
Corresponding author. E-mail: p.smarzewski@pollub.pl

Received (Otrzymano) 06.11.2012

STRESS AND STRAIN ANALYSIS OF REINFORCED CONCRETE BEAM ACCORDING TO PROPOSED METHODOLOGY OF PARAMETER SELECTION OF HIGH STRENGTH CONCRETE

The article presents the analysis of the stress and strain state of reinforced high strength concrete beams with a low level of reinforcement in the process of static deformation in comparison to experimental data, according to the methodology of determining the parameters for the constitutive model of high strength concrete, based on its ultimate uniaxial compressive strength. Three variants of numerical solutions of the BP-1a beam were presented, which are distinguished by their failure surface. Numerical calculations made with the use of the Newton-Raphson method with adaptive descent and Crisfield's arc length method are verified with experimental results. The development of strain for extreme concrete fibres of the compression zone and the development of strain for a longitudinal reinforcement bar in the tension zone at beam's midspan are characterized by excellent agreement in the presented cases.

Keywords: finite element method, reinforced concrete, beam, high strength concrete

ANALIZA STANU ODKSZTAŁCENIA I NAPRĘŻENIA BELKI ŻELBETOWEJ WEDŁUG PROPONOWANEJ METODYKI DOBORU PARAMETRÓW MODELU BETONU WYSOKIEJ WYTRZYMAŁOŚCI

W artykule przedstawiono analizę stanu odkształcenia i naprężenia belki żelbetowej o niskim stopniu zbrojenia wykonanej z betonu wysokiej wytrzymałości w procesie statycznego odkształcania w porównaniu z wynikami eksperymentalnymi według metodyki ustalania parametrów modelu konstytutywnego betonu wysokiej wytrzymałości na podstawie jego wytrzymałości na ściskanie. Przedstawiono trzy warianty rozwiązania numerycznego belki BP-1a zróżnicowane powierzchnią graniczną betonu. Obliczenia numeryczne wykonane metodami Newtona-Raphsona ze spadkiem adaptacyjnym i długości łuku Crisfielda zweryfikowano z wynikami eksperymentalnymi. W prezentowanych przypadkach rozwój odkształceń skrajnych włókien betonu w strefie ściskanej i rozwój odkształceń pręta podłużnego w strefie rozciąganej w środku belki charakteryzuje się doskonałą zgodnością.

Słowa kluczowe: metoda elementów skończonych, żelbet, belka, beton wysokiej wytrzymałości

INTRODUCTION

Strain analysis of a construction element is an important issue for construction mechanics as it allows for safety evaluation and optimal design. The dynamic advancement of computer technologies and new generations of computing software allow the simulation of the nonlinear behaviour of reinforced concrete constructions up to their complete failure with consideration of the material properties, real distribution of the reinforcement and the bond between the concrete matrix and steel bars.

METHODOLOGY OF SELECTING MATERIAL MODEL PARAMETERS

The article presents the analyses of the behaviour of a model reinforced high strength concrete beam in the

process of static deformation. The numeric spatial model of a reinforced concrete beam uses the dimensions of a simply supported rectangular BP-1a beam, analysed and described by Kamińska in her work [1]. Considering the longitudinal symmetry of the elements, the subject of modelling was $\frac{1}{2}$ of a beam, 1700 mm long, 150 mm wide and 300 mm high.

The results of numerical calculations made by means of the Newton-Raphson method with adaptive descent and the definition of Crisfield's arc length are compared to the experimental data [1]. Three numerical solutions of a BP-1a beam are presented in detail in the article [2]. The concrete parameters are described on the basis of concrete strength under uniaxial compression. In the first version of the numerical solution, the model is described by a three parameter failure surface in accordance with the William-Warnke theory [3], and by

the author's own proposal of surface evolution in the function of its strain described in [4]. In the second version of numerical solution, the concrete model is described by a five-parameter failure surface which is compressed and tensed, in accordance with the William-Warnke theory and the laws of its evolution. The material models in the third solution are identical to the first proposal. In the first two variants of the solution the definition of Crisfield's arc length was used [5], whereas, in the third one, the author employed the Newton-Raphson method with adaptive descent [6]. All the numerical calculations were made for a perfectly elastic-plastic model of reinforced steel and an elastic-brittle model of concrete with softening in tension.

ANALYSIS OF STRESS AND STRAIN

In order to observe the strain changes of concrete in the function of load, the author chose a point at the upper edge of the BP-1a beam cross-section, while in order to record the changes in beam deformation in the function of load - the point in the longitudinal bar in the tension zone at the beam midspan was selected. Figure 1 presents the development of strain in the extreme fibres of the concrete compression zone, while Figure 2 presents the relation of strain in the longitudinal bar in the function of load - F at the midspan of the numerical and experimental model of the BP-1 beam.

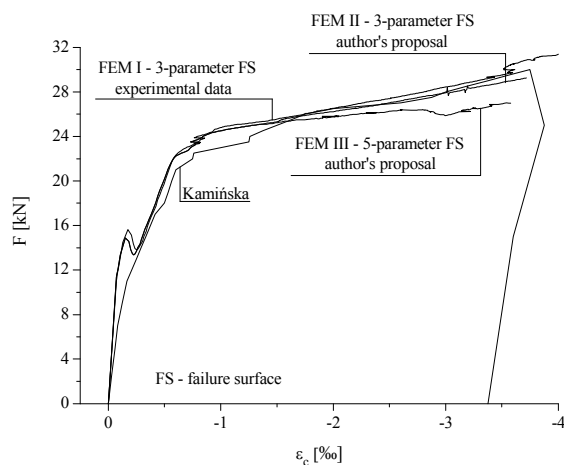


Fig. 1. Comparison of strain development in extreme fibres of concrete compression zone at beam midspan

Rys. 1. Porównanie rozwoju odkształceń w środku belki skrajnych włókien strefy ściskanej betonu

All the graphs of load-strain for both the concrete and the reinforcement at midspan are characterised by conformity in the function graphs of the experimental results. In case of the results obtained by Crisfield's method and the experimental results for construction material strain, the differences can be observed for inelastic stresses. At the moment of reinforcement yielding, a twist in the graphs can be easily observed. In the three graphs obtained by Crisfield's method numerical calculations, one can see a characteristic slight decrease

in load when the first cracking appears. For the experimental graphs, the branches of element unloading were registered after exhausting the potential of the test bench.

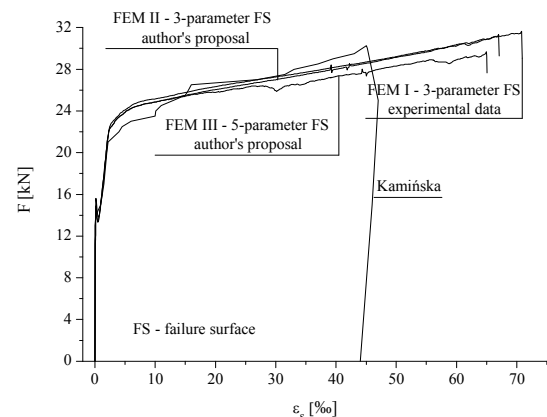


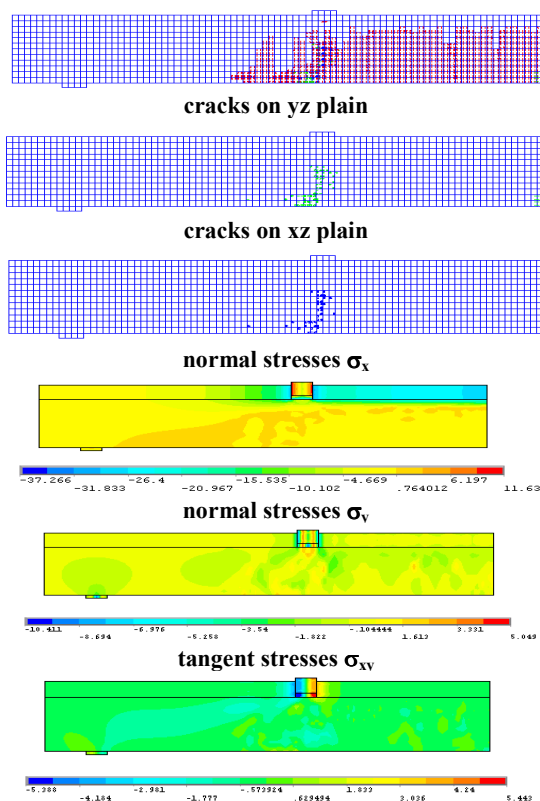
Fig. 2. Comparison of strain development of longitudinal bar in tension zone at beam midspan

Rys. 2. Porównanie rozwoju odkształceń pręta podłużnego strefy rozciąganej w środku belki

Under the load of $F = 14.9$ kN the distribution of stress characteristics for the elastic work of the beam was observed. Yet, at this level of load, the first plastic processes in the concrete occurred, as well as narrow concrete failure along the main reinforcement in the fragment of constant moment. In the remaining part of the beam, the concrete works in the elastic range in both compression and tension.

Further load causes the concrete to undergo a rapid cracking processes in the load zone, which, causes a momentary lapse of force down to $F = 13.3$ kN. The areas of stresses corresponding to the smeared crack regions are regular. With the increase in load, one can observe the approximation of the neutral axis to the extremely compressed concrete fibres. At the load of $F = 21$ kN, the plastification area of the tensing concrete is smaller. The wavy curve of the neutral axis and gradual decrease of the tensed concrete plastification are characteristic for this distribution. Yet, for the load of $F = 25$ kN in the phase of reinforcement yield, one can observe the development of crushing in the compressed concrete plastification zone. For the load of $F_u = 31.3$ kN, in the case of the three parameter failure surface, the beam load was exceeded and the construction was locally crushed in the compressed zone. In the case of the five-parameter failure surface, the load was exceed and local concrete crush happened at the load level of $F_u = 29.7$ kN. At the moment of crush, the neutral axis in both solutions was located close to the compressed edge. The failure cracks propagated virtually across the beam. The development of the crushing process is notably visible in the solution for the five-parameter failure surface. Figure 3 presents the comparison of cracking maps in three perpendicular plains of the BP-1a beam with the distribution of normal and tangent stresses at the same load $F = 23$ kN.

Three-parameter and five-parameter failure surface (Crisfield's arc length method [A-L])summary cracking



Three-parameter failure surface (Newton-Raphson method with adaptive descent [N-R ad]) summary cracking

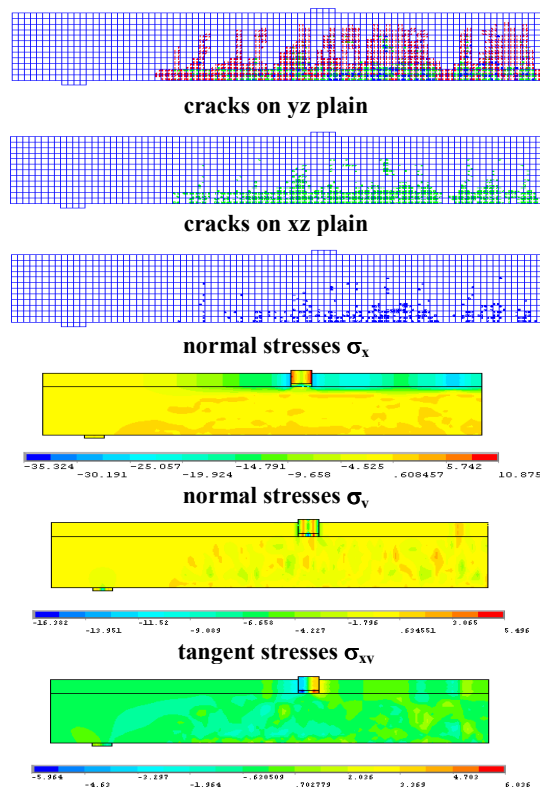


Fig. 3. Maps of smeared cracks in three perpendicular plains and distribution of normal and tangent stresses for load $F = 23$ kN on BP-1a beam

Rys. 3. Zestawienie rys rozmytych w trzech płaszczyznach prostokątnych i rozkładów naprężeń normalnych i stycznych belki BP-1a dla siły $F = 23$ kN

The development of normal compression stresses σ_y was observed above the support and in the zone of load application, and tension stresses σ_y at the beam midspan for the load range from $F = 14.9$ kN up to $F = 25$ kN. The reinforcement yield in both solutions causes even larger stresses in the extreme fibres at the beam axis. At the final stages of loading after the yielding of the reinforcing steel, a further increase in compressing stresses σ_y was observed in the areas above the support, in the load application zone and in the compressed fragment of the beam at the length of pure bending. Yet in both numerical solutions compressing stresses σ_z develop in the extreme fibres of the compressed concrete between the forces cumulated in the final stages of loading. The development of tangent stresses $\sigma_{xy}, \sigma_{yz}, \sigma_{xz}$ in three perpendicular plains agrees with the area of smeared cracks. Normal tensing stresses σ_x and tangent compressing stresses σ_{xy} determine the diagonal direction of the main stresses and determine the formation of diagonal cracks in the support zones. On the other hand, the tangent tensing stresses σ_{yz} and σ_{xz} facilitate the development of concrete cracking in the area of constant moment in the fragment of pure bending and at the level of the main reinforcement along the beam. Figure 4 presents the location of the cross sections in which the distribution of normal stresses σ_x was observed in the concrete matrix and reinforcing steel. Due to the symmetry of the construction, the presented results concern the left part of the analysed BP-1a beam.

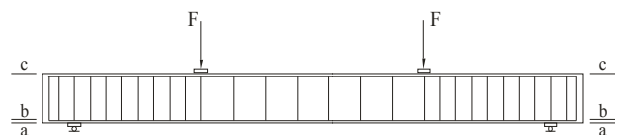


Fig. 4. Scheme of observing sections for distribution of stresses

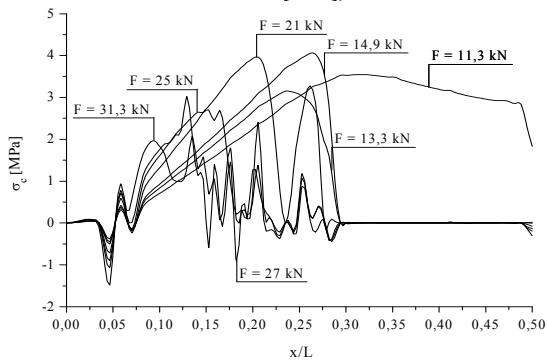
Rys. 4. Schemat usytuowania przekrojów obserwacji stanu naprężenia

The first group of figures presents the distribution of normal stresses σ_c in the concrete matrix along the element. Figure 5 illustrates that distribution of normal stresses σ_c in the a-a section and Figure 6 presents the variation of stresses σ_c in the c-c section.

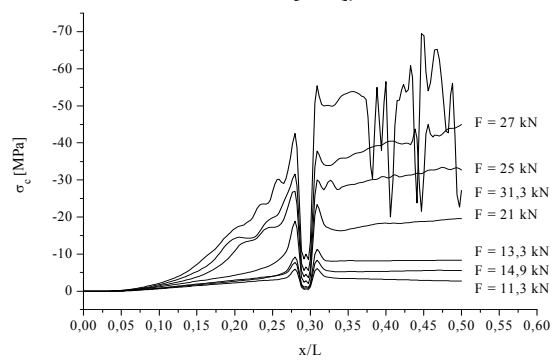
The following group of illustrations concerns graphic imaging of the stresses changeability in the main reinforcement in the b-b section, depending on the external load F . Figure 7 presents the distribution of normal stresses σ_s in the longitudinal bar.

Due to the fact that the distribution of normal stresses σ_s in the main reinforcement along the b-b section obtained by Crisfield's arc length method were virtually identical, Figure 7 presents the changeability of stresses in the longitudinal bar only for the first variant of the numerical solution.

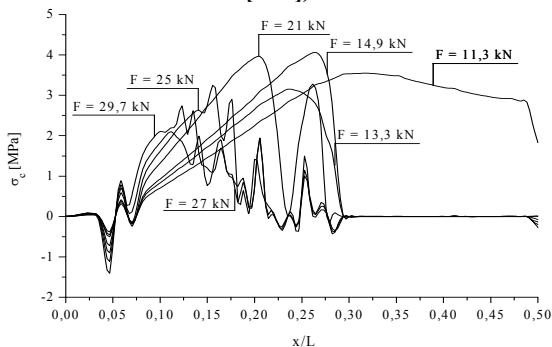
Three-parameter failure surface (Crisfield's arc length method [A-L])



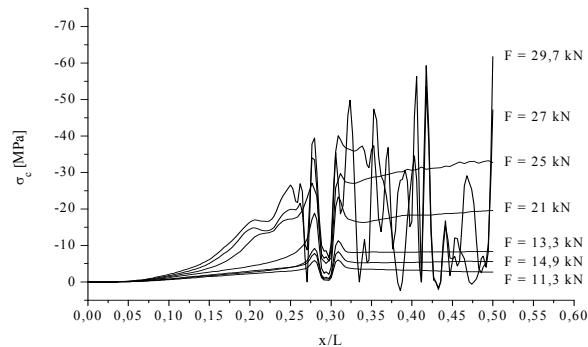
Three-parameter failure surface (Crisfield's arc length method [A-L])



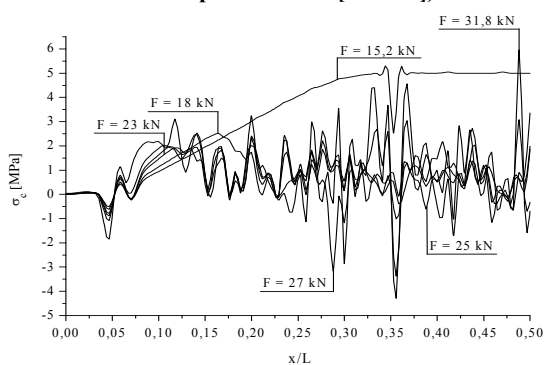
Five-parameter failure surface (Crisfield's arc length method [A-L])



Five-parameter failure surface (Crisfield's arc length method [A-L])



Three-parameter failure surface (Newton-Raphson method with adaptive descent [N-R ad])



Three-parameter failure surface (Newton-Raphson method with adaptive descent [N-R ad])

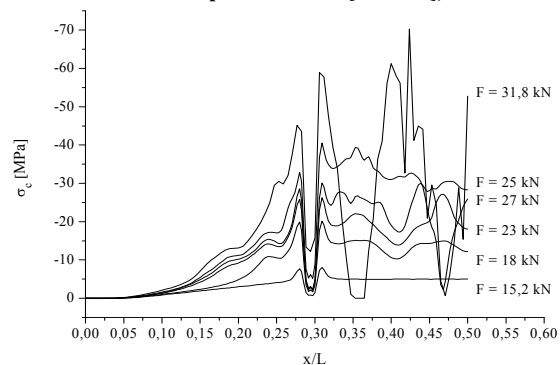


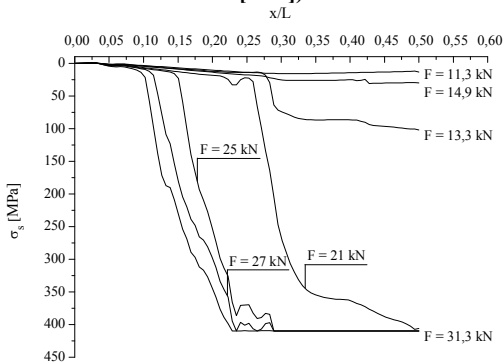
Fig. 5. Distribution of normal stresses σ_c in concrete matrix along a-a section for different values of load

Fig. 6. Distribution of normal stresses σ_c in concrete matrix along c-c section for different values of load

Rys. 5. Rozkład naprężeń normalnych σ_c w materiale matrycy betonowej w przekroju a-a dla różnych poziomów obciążenia

Rys. 6. Rozkład naprężeń normalnych σ_c w materiale matrycy betonowej w przekroju c-c dla różnych poziomów obciążenia

Three-parameter failure surface (Crisfield's arc length method [A-L])



Three-parameter failure surface (Newton-Raphson method with adaptive descent [N-R ad])

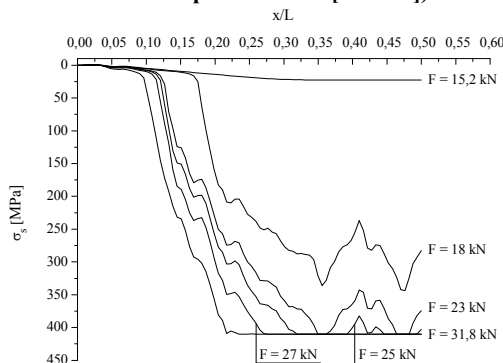


Fig. 7. Distribution of normal stresses σ_s in concrete matrix along b-b section for different values of load

Rys. 7. Rozkład naprężeń normalnych σ_s w zbrojeniu głównym w przekroju b-b dla różnych poziomów obciążenia

SUMMARY

Summarising the presented results, one may conclude that the most probable image of the real work of reinforced concrete bending elements, coherent with the image of processes happening during the work of the reinforced concrete beam described in the work by Szechiński [7], was obtained by the Newton-Raphson method with adaptive descent, which is directly linked to the location and concentration of the smeared areas of cracking. Applying very small but constant increases in load in the nonlinear phase determines the limitation of the failure area. The most significant fact in the obtained numerical solution (N-R ad) is that the distributions of stresses in both the concrete and the main reinforcement are irregular and characterised by abrupt changes in the spots where cracks are formed. The stresses near the cracks increase and they decrease between them. Along with the changes in strains, there are also changes in the natural axis location in the cross section along the beam axis, which, consequently causes abrupt changes in the distribution of stiffness along the element in the spots of cracking. The above statements may be the basis for the theoretical descriptions of the deformations of reinforced concrete beams.

REFERENCES

- [1] Kamińska M.E., Doświadczalne badania żelbetowych elementów prętowych z betonu wysokiej wytrzymałości, KILiW, PAN, Łódź 1999.
- [2] Smarzewski P., Cracking analysis of reinforced concrete beam according to proposed methodology of parameter selection of high strength concrete, *Composites* 2013.
- [3] Willam K.J., Warnke E.P., Constitutive Model for the Triaxial Behavior of Concrete, Proceedings, International Association for Bridge and Structural Engineering, ISMES, Bergamo, Italy 1975, Vol. 19.
- [4] Smarzewski P., Modelowanie mechanizmu zniszczenia belek żelbetowych z betonu wysokiej wytrzymałości, Praca doktorska. Politechnika Lubelska, Lublin 2008.
- [5] Crisfield M.A., Non-linear Finite Element Analysis of Solids and Structures, John Wiley & Sons, Inc., 2000.
- [6] Eggert, G.M., Dawson, P.R., Mathur K.K., An adaptive descent method for nonlinear viscoplasticity, *International Journal for Numerical Methods in Engineering* 1991, 31, 1031-1054.
- [7] Szechiński M., Ugięcia długotrwałe obciążonych belek żelbetowych, Studium porównawcze, Oficyna Wydawnicza Politechniki Wrocławskiej, Wrocław 2000.